Title: Optical Elastography for Micropressure Characterization of Zebrafish Embryonic Cardiac Development

Authors: Anand G. Vaish[1], Yuji Tomizawa[1], David F. Daggett[2] and Kazunori Hoshino[1]

[1]Department of Biomedical Engineering, University of Connecticut.

A.B. Bronwell Building, Room 217

260 Glenbrook Road, Unit 3247

University of Connecticut

[2]Department of Molecular and Cell Biology, University of Connecticut

Biology Physics Building (BPB) 104

91 N. Eagleville Road

Unit-3125

Abbreviated Title: Pressure Characterization of Fish Heart Development

Correspondence:

Kazunori Hoshino

Hoshino@engr.uconn.edu

Conceptualization: A.V, D.D and K.H; Methodology: A.V, D.D and K.H; Formal Analysis: A.V, Y.T and K.H; Resources: K.H and D.D; Writing – original draft preparation: A.V; Writing – review and editing: A.V, D.D and K.H; Project administration and funding acquisition: K.H

Abstract:

The proper formation of the vertebrate embryonic heart relies on various mechanical forces which determine its form and function. Measuring these forces at the microscale of the embryo is a challenge. We propose a new tool utilizing high-resolution optical elastography and stiffness measurements of surrounding tissues to non-invasively track the changes in the pressure exerted by the heart on the neighboring yolk, as well as changes in contractile patterns during early cardiac growth *in-vivo*, using the zebrafish embryo as a model system. Cardiac development was characterized every three hours from 24 hours post-fertilization (hpf) to 30 hpf and compared between wildtype fish and those treated with MS-222, a commonly used fish anesthetic that decreases cardiac contractility. Wildtype embryos from 24 hpf to 30 hpf showed an average yolk indentation pressure of 0.32 mmHg to 0.41 mmHg, respectively. MS-222 treated embryos showed an average yolk indentation pressure of 0.22 mmHg to 0.29 mmHg. Yolk indentation pressure between control and treated embryos at 24 hpf and 30 hpf showed a significant difference ($p < 0.05$). Our method allowed for contractility and pressure evaluation at these early developmental stages, which have not been previously reported in published literature, regardless of sample or imaging modality. This research could lead to a better understanding of heart development and improved diagnostic tools for congenital heart disease.

Key Terms: zebrafish embryo, cardiac development, contractile patterns, optical elastography, blood pressure

Introduction:

The heart is one of the earliest organs to form and function in the vertebrate embryo. In humans, the heartbeat can be assessed seven weeks after gestation. Proper heart formation during embryonic development involves a complex interplay between molecular, cellular, and mechanical signaling pathways. Disturbances to these pathways can cause various defects in cardiac morphogenesis, leading to increased embryo mortality [1]. Research within the last decade has shown that perturbations to the mechanical signaling pathways of the vertebrate embryonic heart can lead to defects in structure and function that resemble congenital heart disease [2]. For example, feedback between the morphological and mechanical properties of developing cardiac tissue and local forces, such as compression or blood shear- have been shown to be mediated by specific molecular and cellular mechanisms [3]. Therefore, the biomechanical properties of the embryonic heart play a significant role in its development, and the quantification of these properties can help differentiate normal and perturbed growth.

The zebrafish has long been a powerful model for investigating the mechanisms of cardiac development due to their genetic tractability, their similarity to humans in early cardiac development, their ability to survive with an impaired circulatory system, their high fecundity, and their optical transparency [4–6]. The developing zebrafish cardiac tissue begins to beat at 24 hours post fertilization (hpf). At this stage, it can be described as a linear heart tube with no valves or chambers present, consisting primarily of the myocardium. As development progresses to 30 hpf, a shift from a pulsatile contractile pattern to a two-stage contractile pattern marks the emergence of

the atrium and ventricle chambers [7]. Many studies in zebrafish have been instrumental in furthering our understanding of the complex interplay between morphological development and biomechanical forces in the heart [8]. However, the specific mechanisms that relate cardiac development and hemodynamic forces are still not fully understood.

Most traditional methods of mechanical characterization are hindered by the microscopic size of the zebrafish embryo heart, which ranges from 100 μm-200 μm during early development. Quantification methods such as uniaxial or biaxial testing have been used to test vessels in the >200 μm range but have not yet been applied to zebrafish and cannot be performed in-vivo [9]. At the microscale, several methods used for cellular mechanical analysis are atomic force microscopy, micro-indentation, and optical tweezers, but these are limited to quantifying a small, localized area of interest [10–12]. For hemodynamic characterization at this scale, only a few methods exist including servo null measurement systems, particle image velocimetry, and computational fluid dynamics [6, 13, 14]. These methods have been used to study endothelial wall shear stress. ventricular deformation, and pressure-volume changes within growing zebrafish embryos, but are generally applied to embryos at later stages of development (>72 hpf) [15, 16]. Servo null measurement systems allow for direct pressure measurements within the embryonic heart but can be difficult to perform, are invasive, and cannot be easily scaled to larger sample sizes. In comparison, particle image velocimetry and computational fluid dynamics are both non-invasive tools for hemodynamic analysis but rely on purely computational approaches.

In this work, we demonstrate a novel tool based on optical elastography combined with micro-cantilever beam manipulation that allows for rapid, non-invasive, label-free in-situ monitoring of passive mechanical properties of the zebrafish heart throughout development by utilizing tissues of known stiffness as a sensor. Specifically, we quantify the deformation of the yolk caused by the relaxation of the embryo heart during a single heartbeat, the yolk indentation pressure, as well as changes in contractile patterns from 24 hpf to 30 hpf. Overall, our tool presents a simple and sensitive method to quantify cardiac function at early developmental stages.

Materials and Methods:

Zebrafish Embryo Collection and Preparation:

Adult male and female zebrafish (Danio rerio) of the wildtype AB strain were separated overnight and then placed together in a 1:2 proportion in breeding tanks at the start of the light cycle the following morning. Fertilized embryos were then collected and staged under light microscopy and embryos in the zygote period were separated. These embryos were then maintained in embryo media (15 mM NaCl, 0.5 mM KCl, 1 mM CaCl2, 0.15 mM KH2PO4, 0.05 mM Na2HPO4,1 mM MgSO4 and 0.84 mM NaHCO3) at 28° C until 24 hpf. Embryos at 24 hpf were dechorionated using #12 watchmaker forceps and transferred onto a glass coverslip with a raised silicone well. The embryos were then embedded in 0.6% agarose solution in embryo media. Each embryo was manipulated into a lateral view using a custom poker device made from fishing line. A total of six embryos were staged in this manner. The raised silicone well

was filled with embryo media for the three control embryos and a 383 μM solution of M2-222 (Sigma Aldrich, MO) diluted in embryo media for the three embryos in the experimental group. Dosage for chronic MS-222 treatment was determined by established anesthetic guidelines and dosages utilized by previously published studies [17, 18]. The staged zebrafish embryos were then placed on a heated imaging stage (BoliOptics, CA) at 28° C. Every hour, the respective solutions were added to the well to keep the volume consistent and replace lost media from evaporation. Agar embedding has been shown to not significantly impact zebrafish embryo physiology, and the use of embryos at the 24 hpf stage minimizes tail extension complications in the morphological analysis [19].

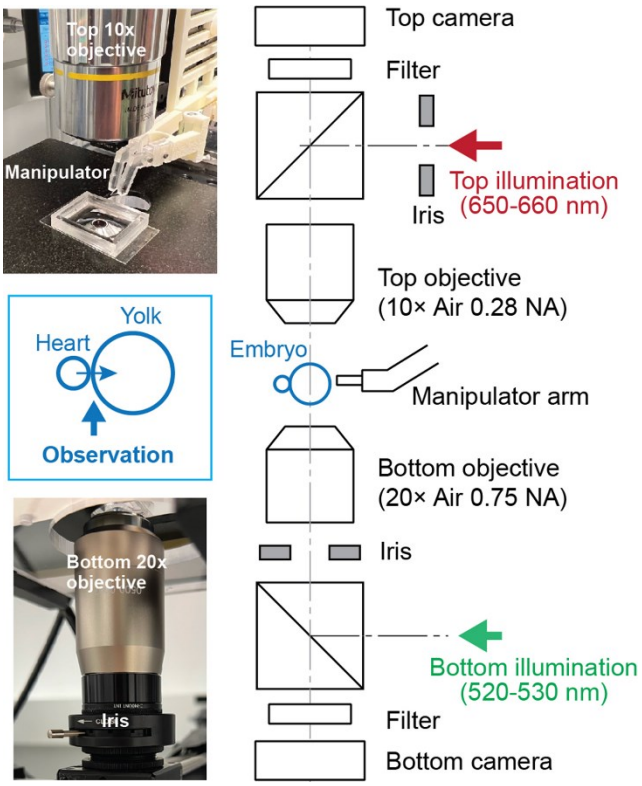

Fig. 1 Experimental setup of image collection. The system comprises a high-resolution bottom microscope and a low-resolution top microscope. Cardiac motion was imaged with the bottom

microscope. The top microscope was used for the yolk stiffness calculation. Embryo was oriented so that the imaging plane was orthogonal to the heart/yolk interface

Image Collection

Figure 1 illustrates the details of the experimental setup. For determining yolk indentation pressure, the bottom microscope consisting of a 5472x3648 pixel Blackfly® S USB3 camera (Teledyne FLIR, OR) and a Nikon CFI Plan APO VC 20 Air 0.75 NA UV Enhanced Microscope Objective lens (Nikon, Japan) were used to capture the heart-yolk interface at higher magnification. A 3 W green LED (520–530 nm) (Chanzon, China) was used for illumination. The top low-resolution microscope, consisting of a 2048 × 1536 pixel 55 fps Chameleon®3 USB3 camera (Teledyne FLIR, OR) and a M Plan Apo 10 × 0.28 NA Long working distance objective lens (Mitutoyo, Japan), was used for the yolk indentation analysis. To reduce vibration on the optical stage, a Vision IsoStationTM Optical Workstation with Pneumatic Isolation (Newport Corporation, CA) was utilized. We oriented the embryo to observe the heart indentation from the bottom view of the experimental setup, i.e., the heart-yolk interface is orthogonal to the image plane (Fig. 1). 1600x1600 pixel videos at 24 frames per second were recorded of cardiac motion every three hours, from 24 hpf to 30 hpf for each embryo (Fig. 2). Each recording was five seconds long, which corresponded to around five heartbeat cycles. The depth of focus was adjusted to best visualize the deformation of the yolk during a heartbeat. Images captured by the bottom microscope are shown in Figure 2a and 2b. The focal depth is defined by the numerical apertures (NA) of the illumination and the observation optics. Each optics system has an iris to reduce the NA, allowing for high-

contrast imaging with a deeper focal depth. Online Resource 1 shows the heart-yolk interface imaged at different objective heights. The interface is sufficiently visible for a range of z =~100 μm, which is larger than the thickness of the heart.

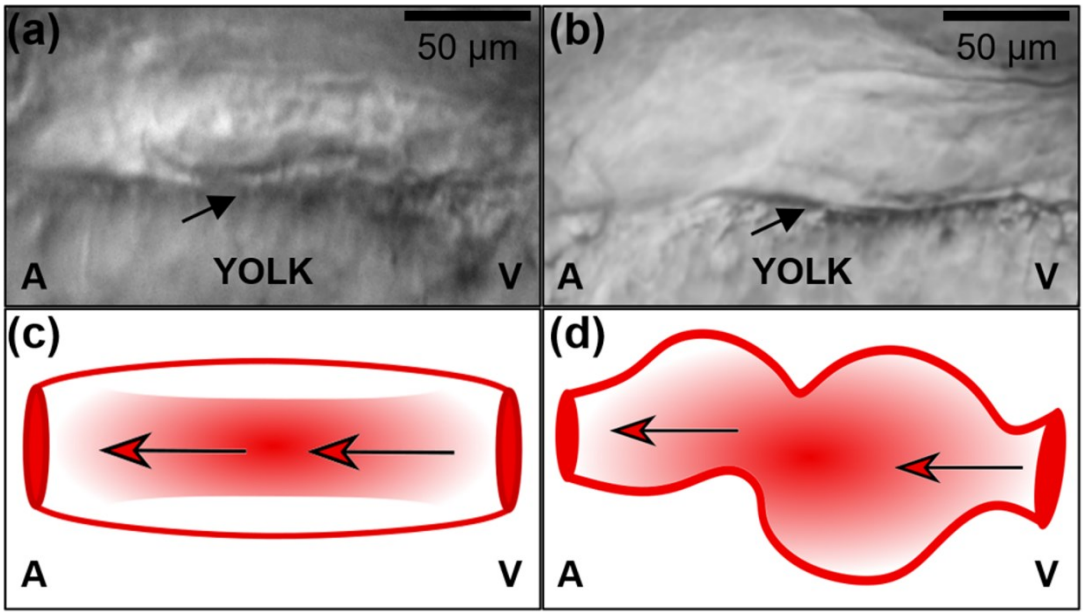

Fig. 2 (a,b) Brightfield images of wildtype zebrafish embryo at 24 and 30 hours post fertilization (hpf). Contrast and brightness have been adjusted to best visualize heart/yolk interface. A and V denote the arterial and venous poles of the heart, respectively. Black arrows point to the heart/yolk interface. (c,d) Cartoon depictions of heart morphology and blood flow direction at these stages. A and V denote the arterial and venous poles of the heart respectively

MATLAB Optical Elastography Analysis:

Videos of the embryonic heart were processed to create a TIFF file containing all the image frames. Before performing the image-based deformation analysis [20], the contrast and brightness of the images were optimized for image analysis. For this analysis, a total of 10 feature points along the heart-yolk interface were chosen. Each of

these points was characterized as a node, which defines a target area and a scan area for optical tracking, Fig. 3.

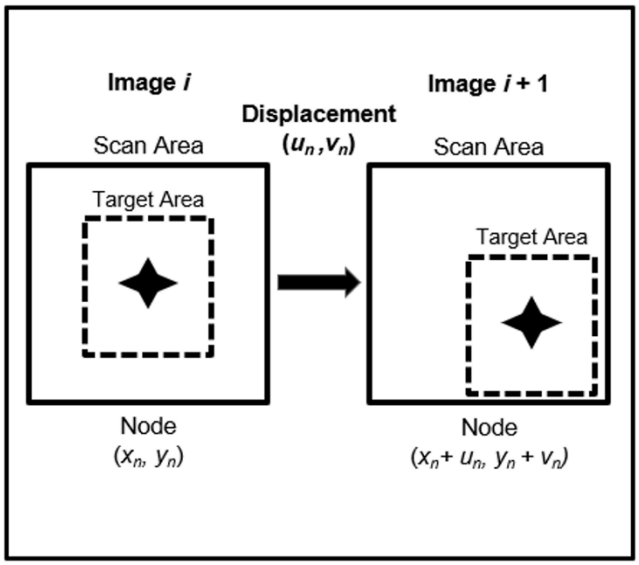

Fig. 3 Representation of feature tracking using MATLAB image analysis. Consecutive frames are searched incrementally for the node defined by the target area. Nodal displacement per frame can then be calculated

The target area was 120x120 pixels, and the scan area was 140x140 pixels. Using the first frame *i*, the program creates a unique pattern for each node based on the pixel intensities of the target area. The scan area was then searched incrementally on the consecutive frame *i* +1 to determine the best match of the target area. This was performed through normalized cross-correlation at every increment. The area with the highest cross-correlation was determined to be the optimally matched area on frame *i* + 1, and this area was updated to be the new target area and used for the search on frame *i* + 2. Therefore, frame by frame, the program searches a defined area around the original target area, looking for the most similar value to the original value. This allows

for the quantification of nodal displacement frame by frame throughout the cardiac cycle.

Yolk Stiffness Quantification

In previous studies, we have made a 3D-printed flexure micro tweezer system which utilizes force-sensing microcantilever beams [21]. We have used this system in conjunction with image-tracking analysis to characterize multicellular tumor spheroids [22, 23]. A recent focus of our studies has been the mechanical characterization of the zebrafish embryonic tissues [24, 25]. To measure the Young's Modulus of the embryo yolk, microcantilever beam manipulation was performed on four zebrafish embryos at 30 hpf. Embryos at 30 hpf were dechorionated using #12 watchmaker forceps and transferred onto a glass coverslip with a raised silicone well filled with embryo media. MS-222 solution at 4g/ml was added dropwise to the well until no embryo movement was observed. Stiffness calculation of the embryo yolk was performed using microcantilever beam indentation on the yolk as shown in **Fig. 4b**. The compression rate used for this analysis was ten compression steps with a one-second interval between steps. The custom MATLAB image-tracking program was utilized to determine the displacement (μ) of the microcantilever beams in response to sample compression. A video of the image-tracking analysis for yolk stiffness measurement is shown in Online Resource 2. The calculated displacement and the spring constant (K) of the microcantilever beam (1.03×10^{-2} N/m) was used to determine the force (F) applied to the embryo. The calculated force was then utilized to determine the stiffness of the sample using the cantilever bending equation referenced in the previously reported

study. The Poisson's Ratio of the yolk was set to 0.5, with the assumption made that it acts as an incompressible isotropic material deforming elastically. This analysis follows basic Hertzian contact mechanics that has been well established in biomechanical characterization. To calculate the stiffness using Hertzian contact mechanics, the assumption is made that a viscoelastic material can be treated as quasistatic if the compression rate is slow enough.

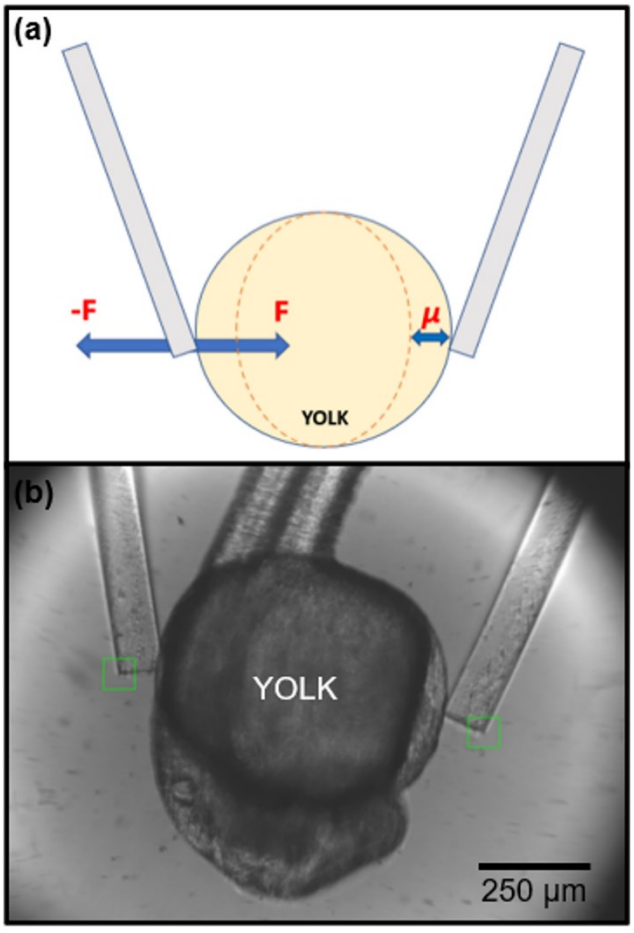

Fig. 4 Microcantilever beam manipulation to determine yolk stiffness of an embryo at 30 hpf. (a) Cartoon representation of deformation of the beam and the yolk to measure yolk stiffness. (b) Image from MATLAB image analysis tool showing embryo yolk being compressed by microcantilever beams. Green

squares on the microcantilever beams represent node locations for image tracking. See Online Resource 2 for video of yolk stiffness measurement

Yolk Indentation Pressure Quantification and Contractile Pattern Visualization

Hertzian Contact Theory for contact between Two Elastic Bodies with Curved Surfaces was used to calculate indentation pressure [26]. For our model, we assumed a rigid cylindrical indenter compressing a significantly larger elastic cylinder, yielding the following equations.

$$\frac{1}{E^*} = \frac{1-\nu^2}{E_{yolk}} \quad \textbf{(1)}$$

$$F = \frac{\pi}{4} E^* L d \quad \textbf{(2)}$$

$$P = \sqrt{\frac{E^* F}{\pi L R}} \quad \textbf{(3)}$$

In these equations. E_{yolk}, ν, L, d, F, R, and P are equal to the Elastic Modulus of the material being indented, Poisson's Ratio of the material being indented, length of the indenter, displacement depth of the indenter, force of the indenter, radius of indenter, and pressure, respectively. Applying our image analysis method to these equations, we can calculate the indentation pressure. We validated this approach by performing a phantom experiment using a silicone elastomer of known stiffness and acrylic indenter with known force to compare against the results of the Hertzian Model values. A Polydimethylsiloxane (PDMS) piece (3 MPa) was compressed with an acrylic cylindrical indenter (Diameter = 60 μm, Length = 300 μm), where the PDMS piece represented the embryo yolk, and the acrylic cylinder represented the heart. The acrylic cylinder was attached to a micro loadcell with micro strain gauges (SS-060-040-2500-PM, Micron Technology, Boise, ID, USA) and a piezoelectric actuator (APF710,

Thorlabs, Newton, New Jersey). We applied a 1 Hz, 8 μm (p-p) sinusoidal indentation on the PDMS elastomer and measured the amplitude using the same optical system we used for yolk indentation analysis. See Figure 5a for the experimental setup of the phantom indentation and Figure 5b for an image of the image analysis of PDMS deformation. For analysis, a total of three indentation cycles were measured. The average indentation force measured by the force gauge was 5.59 mN. The average indentation force calculated using the Hertzian Model was 5.21 mN. Therefore, error of our measurement system was well within 10%.

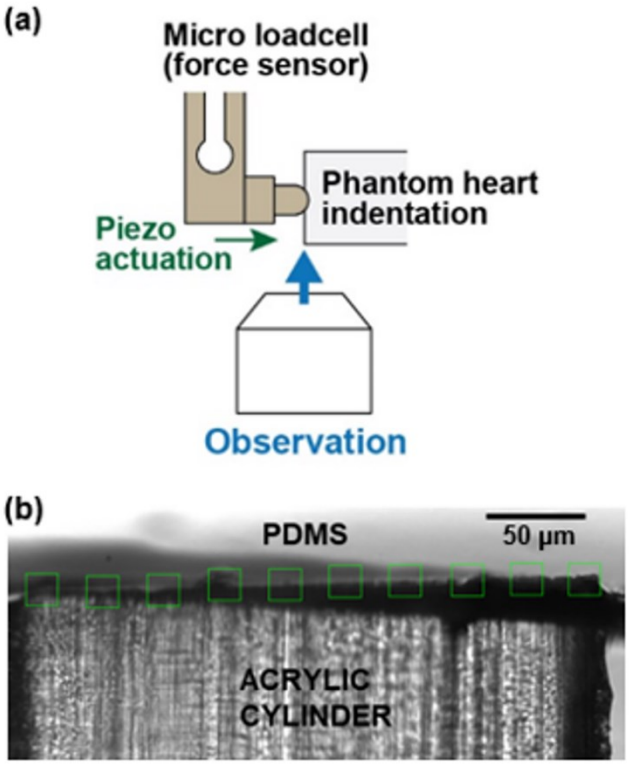

Fig. 5 Validation of the Image-based Hertzian Model for Yolk Deformation Analysis. (a) Experimental Setup of Phantom Indentation. PDMS elastomer was indented by the cylindrical acrylic piece. Indentation force was measured by a micro loadcell with micro strain gauges. (b) Image tracking analysis of PDMS

deformation. 10 tracking nodes were chosen at the PDMS/Indenter interface and the indentation force was calculated

Having validated this method, we modeled the contact between the heart and yolk as 2 parallel cylinders in contact, Fig. 6a and Fig. 6c. A total of 10 Nodes, visually represented as green squares, were manually selected along the heart-yolk interface for image tracking analysis, Fig. 6b. With the calculated elastic modulus of the yolk from the above method, the equivalent elastic modulus of the yolk and heart in contact was calculated using Eq.1. For this analysis we treated the heart as a rigid indenter, so only the elastic modulus of the yolk was used to calculate the equivalent elastic modulus (E^*). The yolk indentation force was calculated using Eq. 2. Using the MATLAB image tracking method, each node's position along the heart-yolk interface during a single heartbeat was tracked. Then the max displacement of each node in the yolk direction during one heartbeat was plotted against its position along the heart. This data was then integrated using the "trapz" function in MATLAB to determine the total yolk area indented by the heart, Fig. 6d. This calculated area was equivalent to the product of the length (L) and indentation depth (d) seen in Eq. 2. To calculate yolk indentation pressure, the radius of each embryo heart was measured using MATLAB and the average radius of the three embryos per timepoint and condition was calculated. The length (L) in Eq. 3 was determined for each embryo heart by taking the distance between the first and last node used during analysis. Yolk indentation pressure was then calculated using Eq. 3. All analyses were performed in MATLAB.

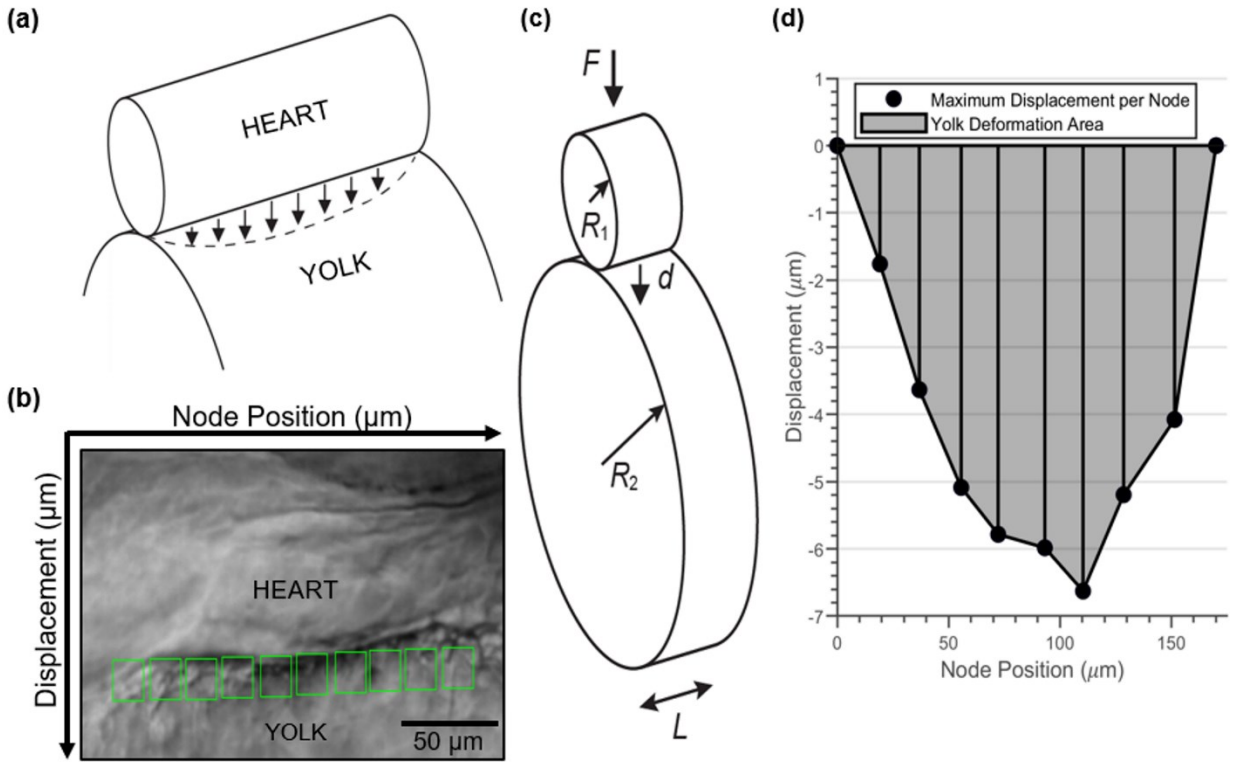

Fig. 6 Calculation of Yolk Indentation Pressure. Hertzian Contact Theory for contact between Two Elastic Bodies with Curved Surfaces was used to calculate yolk indentation pressure. (a) The contact between the heart and yolk was modeled as 2 parallel cylinders in contact. (b) 10 Nodes represented as green squares were placed along the heart-yolk interface for image tracking analysis. (c) Description of parameters used in Hertzian Model analysis: *R1* and *R2* represent the radius of the heart and yolk respectively, *F* is the indentation force of the heart, *d* is the measured yolk indentation and *L* is the length of heart/yolk interface. (d) Integration of maximum yolk deformation area during one heartbeat for pressure calculation. See Online Resource 3 for a video of yolk deformation image tracking analysis of an untreated embryo at 30 hpf

Results:

Contractile Patterns Change During Early Cardiac Development

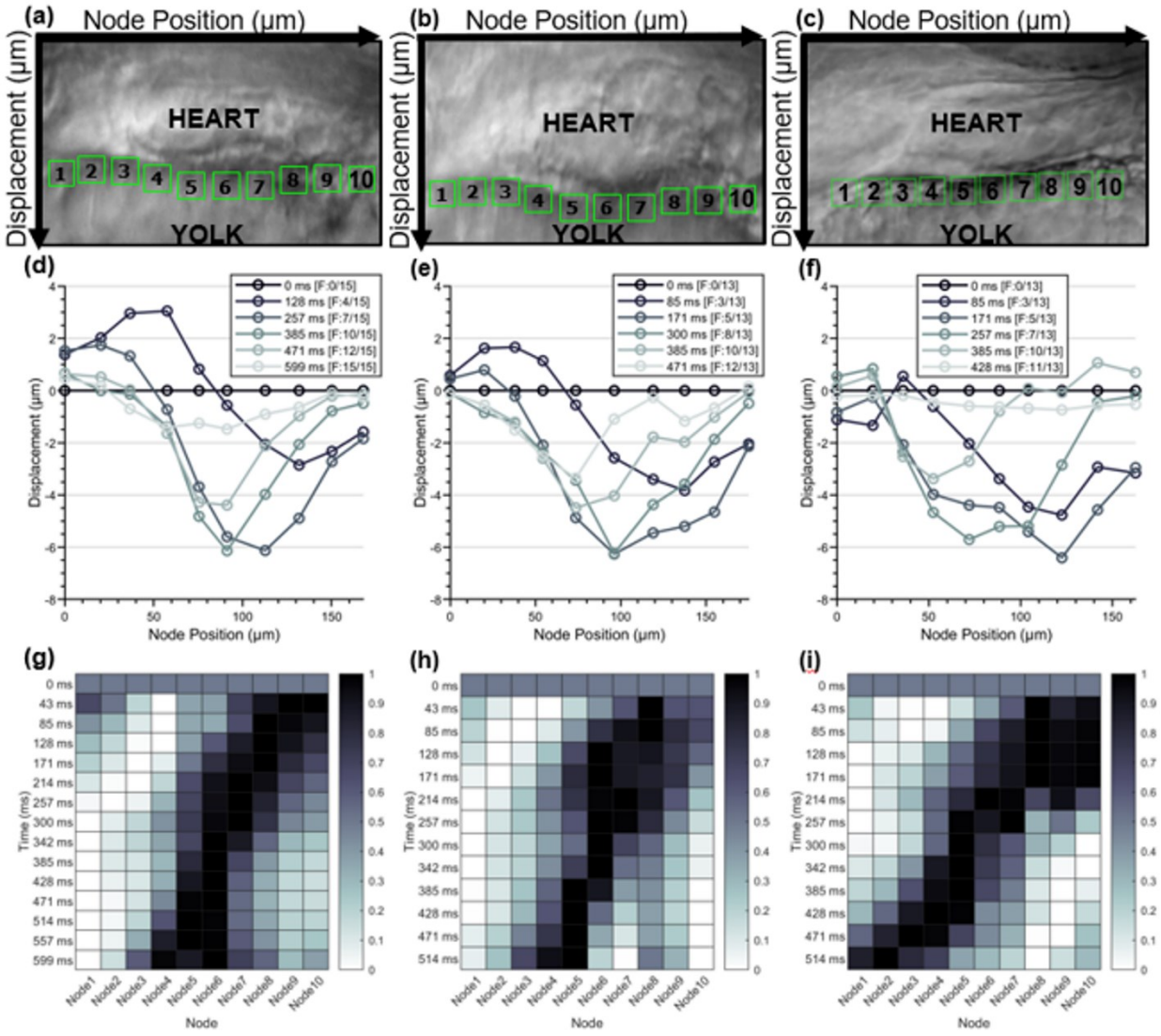

Fig. 7 Heart contractile patterns at 24 hpf, 27 hpf and 30 hpf. (a-c) Images of the 10 nodes used for analysis. Nodes were manually chosen along the heart/yolk interface. (d-f) Plots of nodal displacement (μm) of 6 frames during a single heartbeat of an untreated embryo at 24 hpf, 27 hpf, and 30 hpf. Nodal displacement for all frames were standardized to the first frame. Positive and negative displacement indicate movement away from and towards the yolk, respectively. Node 1 is at the arterial pole of the heart and Node 10 is at the venous pole of the heart. Note a single central peak of deformation at 24 hpf compared to two peaks on opposite sides at 30 hpf. (g-i) Heatmap plots of normalized max displacement per frame during a single heartbeat of an untreated embryo at 24 hpf, 27 hpf, and 30 hpf. Each frame's nodes were normalized to the max nodal displacement of that frame. Darker colors indicate displacement

towards the yolk while lighter colors indicate displacement away from the yolk. Note that the area of max displacement stays central at 24 hpf but travels fully across the heart at 30 hpf

To show changes in the contractile patterns during development from 24 hpf to 30 hpf, the displacement of each node per frame was determined. There is a clear change in contractile patterns from 24 hpf to 30 hpf. Shown in Fig. 7d and Fig. 7g, at 24 hpf the heart begins to deform the yolk at the venous pole and travels centrally increasing in amplitude. The arterial pole of the heart only displaces in the positive direction which is not seen in later timepoints. At 27 hpf, the contractile patterns are still like those at 24 hpf, with a single central peak of negative displacement, but the positive displacement in the arterial pole has decreased and negative displacement has begun to occur in this region, Fig. 7e and Fig. 7h. At 30 hpf, two clear peaks of negative displacement, one towards the venous pole and the other towards the arterial pole are present. This wave travels from pole to pole, with almost no positive displacement occurring during the heartbeat, Fig. 7f and Fig. 7i.

Yolk Indentation Pressure as a Measure of Cardiac Function

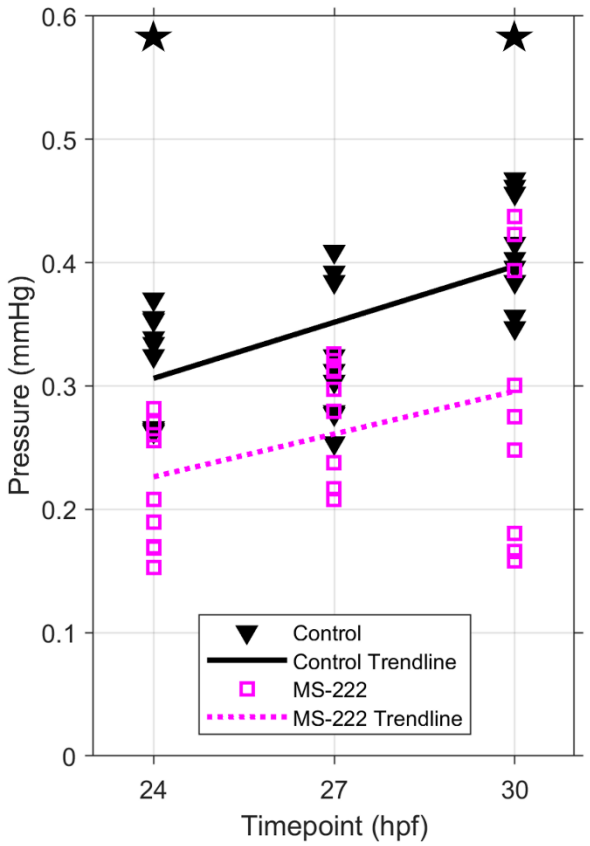

Fig. 8 Plot of Yolk Indentation Pressure (mmHg) of control and MS-222 treated zebrafish embryos at 24 hpf, 27 hpf, and 30 hpf. 3 heartbeats from each control (N=3) and treated (N=3) embryos at each timepoint were used for analysis. Results of linear regression: Control Trendline: $y = 0.0152x – 0.0575$, $R^2 = 0.37$; MS-222 Treated Trendline: $y = 0.0116x – 0.0515$, $R^2 = 0.14$. Black stars above 24 hpf and 30 hpf represent significant difference in yolk indentation pressure between conditions at that timepoint ($p < 0.05$)

To evaluate our tool's ability to discern between normal and altered cardiac function, yolk indentation pressure of wildtype and MS-222 treated embryos from 24 hpf to 30 hpf were compared. Overall, yolk indentation pressure increases over time for both the control and treated embryos. A 2-sample t-test (MATLAB 2023a) was performed between control and treated embryos at each timepoint. A significant difference in mean yolk indentation pressure was found between control and treated

embryos at both 24 hpf and 30 hpf ($p < 0.05$). Furthermore, a 2-sample t-test was performed on yolk indentation pressure between 24 hpf and 30 hpf for each condition. A significant difference in pressure was found between 24 hpf and 30 hpf for control embryos but not MS-222 treated embryos.

Discussion:

We developed a tool to quantify the pressure exerted from the heart on the surrounding tissues as well as the contractile patterns of the embryonic zebrafish heart. By measuring the yolk indentation occurring during a single heartbeat, we were able to quantify the force and pressure exerted by the zebrafish heart *in-vivo*. This measurement allowed for an *in-vivo* indicator of cardiac function for the developing embryonic heart after its very first heartbeat.

This study demonstrates that in principle, due to the favorable optical qualities of the zebrafish embryo, this microscopy tool can be easily applied to better understand the mechanical parameters of cardiac development. The quantification of such parameters could help better differentiate mutant phenotypes which affect cardiac function, potentially allowing for a more precise analysis of the underlying deficiencies. Many studies on cardiac mutant phenotypes utilize well-established markers of proper heart development such as ventricular shortening fraction, beats per minute, and red blood cell flow rate [27]. Our new marker, yolk indentation pressure, represents a combination of several cardiac factors including cardiac contractile and relaxation forces, stiffness of the heart tissue, and vessel area, which allows for a holistic

measurement of cardiac function. We validated this claim by comparing yolk indentation pressure measurements from untreated wildtype embryos to MS-222 treated embryos.

The results of the analysis show a moderate positive linear trend in pressure from 24 hpf to 30 hpf for control embryos and a weak positive linear trend for treated embryos, Fig. 8. This increase in pressure over time is expected as the heart grows and is required to accommodate the development of vasculature throughout the embryo. During the timepoints analyzed, the heart remains a relatively linear tube in direct contact with the yolk. Therefore, the pressure measured at the site of yolk deformation should be a good estimate of the change in pressure during diastole of the embryonic heart. Furthermore, this method of analysis was sensitive enough to detect a significant difference in pressure between the treatment and control groups. MS-222 has been previously shown to decrease heart contractility within the embryonic heart [28], and our results demonstrate that this tool is sensitive enough to detect that effect on yolk indentation pressure.

A thorough literature review revealed that blood pressure measurements at this initial stage of development have not been published before. Although we could find no previously published results on embryonic blood pressure at the stages we investigated, our values appear to be consistent with those reported for subsequent stages. One study utilizing servo-null measurements at 48 hpf detailed values of ventricular blood pressure of 0.49 mmHg [29]. Another study at 48 hpf concluded that physiological blood pressures at this stage are likely below 2 mmHg [14]. Finally, a separate study at 72 hpf reported a mean arterial blood pressure of 0.37 mmHg in the ventral aorta [30]. Due to the difference in methods and timepoints measured, a direct comparison cannot be

made with our measured values, however, these values are quite close to our average yolk indentation pressure value of 0.41 mmHg at 30 hpf. Unlike our method which measures deformation across the entire heart, servo-null measurements provide information for a localized region. This along with the development of cardiac chambers and valves that occur between 30 hpf to 48 hpf could also explain the difference in pressure measurements. Overall, our tool measured physiological pressures which are in line with current published data.

The exact pumping mechanism of the early embryonic zebrafish heart is still not fully understood [31]. When the developing cardiac tube begins to beat at 24 hpf, its contractile pattern is a single wave traveling from the venous to arterial end of the heart. This contrasts with the pumping mechanism of the further developed two chamber heart, whose chambers pump sequentially. These changes in pumping mechanisms have been modeled with 4D computational fluid dynamic studies at later stages in heart development (>72 hpf) [32, 33]. Our method can help better understand this change in pumping mechanics by helping to visualize the contractile patterns of the growing heart, as shown in Fig. 7. Looking at the changes in contractile mechanics from 24 hpf to 30 hpf, the heart initially starts off with a single pole of contraction that begins at the venous end of the heart and travels only to the middle of the heart tube. This contrasts with the pattern at 30 hpf which shows two poles of contraction with the beat traveling from the venous end of the heart all the way to the opposite arterial end of the heart. At this timepoint, the venous and arterial poles of the heart contract sequentially without any valve formation present. The emergence of this contractile pattern may thus be an important marker as a hallmark of proper cardiac development. Therefore, the

application of this tool to quantify the contractile patterns of the growing embryo heart can help better understand normal and perturbed pumping behavior.

Our tool has one main limitation that there must be contact between the heart and the yolk for pressure measurement to occur. This limits the use of our tool during later stages of heart development, as the yolk decreases in size and the heart shifts away from the yolk. Therefore, this tool is best utilized for measuring yolk indentation pressure from 24 hpf to 36 hpf but can measure the contractile patterns of the heart throughout later timepoints as well. As our tool is non-invasive and label-free it can be directly applied with other established hemodynamic measurement methods such as particle image velocimetry or 4D computational fluid dynamics for a complete observation and characterization of the embryonic heart. Continuing, the embryo can be removed from the agarose mounting after 36 hpf to allow for other approaches of late-stage assessment, such as servo null system measurements.

In conclusion, we developed a new method to study embryonic cardiac development in zebrafish. We have shown a significant difference in yolk indentation pressure over the course of 6 hours of cardiac development, as well as between untreated and MS-222 treated embryos. Our method allowed for contractility and pressure evaluation at these early developmental stages, which have not been previously reported in published literature, regardless of sample or imaging modality. Furthermore, the tool can be combined with other standard image-based analysis methods to allow for better characterization of cardiac mutant phenotypes, which can help better understand the relationship between mechanical forces and heart

development. In the future, our tool could be used in conjunction with fetal echocardiography to better quantify human embryonic heart development.

Acknowledgments:

The authors thank the National Science Foundation for funding (CCSS-1809047, CAREER-1942518, and IIBR-2223957).

Conflict of Interest:

The authors declare that they have no conflict of interest.

References:

1. Keller BB, Kowalski WJ, Tinney JP, Tobita K, Hu N (2020) Validating the Paradigm That Biomechanical Forces Regulate Embryonic Cardiovascular Morphogenesis and Are Fundamental in the Etiology of Congenital Heart Disease. Journal of Cardiovascular Development and Disease 7:23. https://doi.org/10.3390/jcdd7020023

2. Lindsey SE, Butcher JT, Yalcin HC (2014) Mechanical regulation of cardiac development. Front Physiol 5:. https://doi.org/10.3389/fphys.2014.00318

3. Hsu JJ, Vedula V, Baek KI, Chen C, Chen J, Chou MI, Lam J, Subhedar S, Wang J, Ding Y, Chang C-C, Lee J, Demer LL, Tintut Y, Marsden AL, Hsiai TK (2019) Contractile and hemodynamic forces coordinate Notch1b-mediated outflow tract valve formation. JCI Insight 4:e124460. https://doi.org/10.1172/jci.insight.124460

4. Bakkers J (2011) Zebrafish as a model to study cardiac development and human cardiac disease. Cardiovasc Res 91:279–288. https://doi.org/10.1093/cvr/cvr098

5. Brown DR, Samsa LA, Qian L, Liu J (2016) Advances in the Study of Heart Development and Disease Using Zebrafish. Journal of Cardiovascular Development and Disease 3:13. https://doi.org/10.3390/jcdd3020013

6. Hu N, Sedmera D, Yost HJ, Clark EB (2000) Structure and function of the developing zebrafish heart. The Anatomical Record 260:148–157. https://doi.org/10.1002/1097-0185(20001001)260:2<148::AID-AR50>3.0.CO;2-X

7. Kimmel CB, Ballard WW, Kimmel SR, Ullmann B, Schilling TF (1995) Stages of embryonic development of the zebrafish. Developmental Dynamics 203:253–310. https://doi.org/10.1002/aja.1002030302

8. Sidhwani P, Yelon D (2019) Fluid forces shape the embryonic heart: insights from zebrafish. Curr Top Dev Biol 132:395–416. https://doi.org/10.1016/bs.ctdb.2018.12.009

9. Zhang R, Gashev AA, Zawieja DC, Davis MJ (2007) Length-tension relationships of small arteries, veins, and lymphatics from the rat mesenteric microcirculation. American Journal of Physiology-Heart and Circulatory Physiology 292:H1943–H1952. https://doi.org/10.1152/ajpheart.01000.2005

10. Lekka M (2016) Discrimination Between Normal and Cancerous Cells Using AFM. BioNanoSci 6:65–80. https://doi.org/10.1007/s12668-016-0191-3

11. Plodinec M, Loparic M, Monnier CA, Obermann EC, Zanetti-Dallenbach R, Oertle P, Hyotyla JT, Aebi U, Bentires-Alj M, Lim RYH, Schoenenberger C-A (2012) The nanomechanical signature of breast cancer. Nature Nanotech 7:757–765. https://doi.org/10.1038/nnano.2012.167

12. Zhang H, Liu K-K (2008) Optical tweezers for single cells. Journal of The Royal Society Interface 5:671–690. https://doi.org/10.1098/rsif.2008.0052

13. Malone MH, Sciaky N, Stalheim L, Hahn KM, Linney E, Johnson GL (2007) Laser-scanning velocimetry: A confocal microscopy method for quantitative measurement of cardiovascular performance in zebrafish embryos and larvae. BMC Biotechnology 7:40. https://doi.org/10.1186/1472-6750-7-40

14. Gendernalik A, Zebhi B, Ahuja N, Garrity D, Bark D (2020) In Vivo Pressurization of the Zebrafish Embryonic Heart as a Tool to Characterize Tissue Properties During Development. Annals of biomedical engineering 49:. https://doi.org/10.1007/s10439-020-02619-5

15. Salehin N, Villarreal C, Teranikar T, Dubansky B, Lee J, Chuong C-J (2021) Assessing Pressure-Volume Relationship in Developing Heart of Zebrafish In-Vivo. Ann Biomed Eng 49:2080–2093. https://doi.org/10.1007/s10439-021-02731-0

16. Salehin N, Teranikar T, Lee J, Chuong C-J (2023) Ventricular anisotropic deformation and contractile function of the developing heart of zebrafish in vivo. Developmental Dynamics 252:247–262. https://doi.org/10.1002/dvdy.536

17. Félix LM, Luzio A, Themudo M, Antunes L, Matos M, Coimbra AM, Valentim AM (2018) MS-222 short exposure induces developmental and behavioural alterations in zebrafish embryos. Reproductive Toxicology 81:122–131. https://doi.org/10.1016/j.reprotox.2018.07.086

18. Matthews M, Varga ZM (2012) Anesthesia and Euthanasia in Zebrafish. ILAR Journal 53:192–204. https://doi.org/10.1093/ilar.53.2.192

19. Muntean BS, Horvat CM, Behler JH, AbouAlaiwi WA, Nauli AM, Williams FE, Nauli SM (2010) A Comparative Study of Embedded and Anesthetized Zebrafish in vivo on Myocardiac Calcium Oscillation and Heart Muscle Contraction. Front Pharmacol 1:. https://doi.org/10.3389/fphar.2010.00139

20. Jaiswal D, Tang-Schomer MD, Sood D, Kaplan DL, Hoshino K (2018) Nondestructive, Label-Free Characterization of Mechanical Microheterogeneity in Biomimetic Materials. ACS Biomater Sci Eng 4:3259–3267. https://doi.org/10.1021/acsbiomaterials.8b00286

21. Almeida A, Andrews G, Jaiswal D, Hoshino K (2019) The Actuation Mechanism of 3D Printed Flexure-Based Robotic Microtweezers. Micromachines (Basel) 10:470. https://doi.org/10.3390/mi10070470

22. Jaiswal D, Moscato Z, Tomizawa Y, Claffey KP, Hoshino K (2019) Elastography of multicellular spheroids using 3D light microscopy. Biomed Opt Express 10:2409–2418. https://doi.org/10.1364/BOE.10.002409

23. Jaiswal D, Cowley N, Bian Z, Zheng G, Claffey KP, Hoshino K (2017) Stiffness analysis of 3D spheroids using microtweezers. PLOS ONE 12:e0188346. https://doi.org/10.1371/journal.pone.0188346

24. Tomizawa Y, Dixit K, Daggett D, Hoshino K (2019) Biocompatible Cantilevers for Mechanical Characterization of Zebrafish Embryos using Image Analysis. Sensors 19:1506. https://doi.org/10.3390/s19071506

25. Tomizawa Y, Daggett DF, Zheng G, Hoshino K (2023) Light microscopy-based elastography for the mechanical characterization of zebrafish somitogenesis. Journal of Biophotonics 16:e202200238. https://doi.org/10.1002/jbio.202200238

26. Popov VL (2010) Rigorous Treatment of Contact Problems – Hertzian Contact. In: Popov VL (ed) Contact Mechanics and Friction: Physical Principles and Applications. Springer, Berlin, Heidelberg, pp 55–70

27. Yalcin HC, Amindari A, Butcher JT, Althani A, Yacoub M (2017) Heart function and hemodynamic analysis for zebrafish embryos. Developmental Dynamics 246:868–880. https://doi.org/10.1002/dvdy.24497

28. Denvir MA, Tucker CS, Mullins JJ (2008) Systolic and diastolic ventricular function in zebrafish embryos: Influence of norepenephrine, MS-222 and temperature. BMC Biotechnology 8:21. https://doi.org/10.1186/1472-6750-8-21

29. Xu X, Meiler SE, Zhong TP, Mohideen M, Crossley DA, Burggren WW, Fishman MC (2002) Cardiomyopathy in zebrafish due to mutation in an alternatively spliced exon of titin. Nat Genet 30:205–209. https://doi.org/10.1038/ng816

30. Kopp R, Schwerte T, Pelster B (2005) Cardiac performance in the zebrafish breakdance mutant. Journal of Experimental Biology 208:2123–2134. https://doi.org/10.1242/jeb.01620

31. Sharifi A, Gendernalik A, Garrity D, Bark D (2021) Valveless pumping behavior of the simulated embryonic heart tube as a function of contractile patterns and myocardial stiffness. Biomech Model Mechanobiol 20:2001–2012. https://doi.org/10.1007/s10237-021-01489-7

32. Cairelli AG, Chow RW-Y, Vermot J, Yap CH (2022) Fluid mechanics of the zebrafish embryonic heart trabeculation. PLOS Computational Biology 18:e1010142. https://doi.org/10.1371/journal.pcbi.1010142

33. Foo YY, Pant S, Tay HS, Imangali N, Chen N, Winkler C, Yap CH (2020) 4D modelling of fluid mechanics in the zebrafish embryonic heart. Biomech Model Mechanobiol 19:221–232. https://doi.org/10.1007/s10237-019-01205-6